https://doi.org/10.5194/egusphere-2023-1762
Preprint. Discussion started: 2 August 2023

Lake Ice Break-Up in Greenland: Timing and Spatio-Temporal Variability

Christoph T. Posch[1], Jakob Abermann[1], Tiago M. Ferreira da Silva[1]

[1]Institute of Geography and Regional Science, University of Graz, Graz, A-8010, Austria

Correspondence to: Christoph T. Posch (christoph.posch@edu.uni-graz.at)

Abstract. Synthetic aperture radar (SAR) data from the Sentinel-1 (S1) mission with its high temporal and spatial resolution allows for an automated detection of lake ice break-up timings from surface backscatter differences across South (S), Southwest (SW) and Northwest (NW) Greenland (< 71° N latitude) during the period 2017 to 2021. Median break-up dates of the 563 studied lakes range between 8 June and 10 July, being earliest in 2019 and latest in 2018. There is a strong correlation between break-up date and elevation, while no relationship with latitude and lake area could be observed. Lake-specific median break-up timings for 2017-2021 increase (i.e., are later) by 3 days per 100 m elevation gain. When assuming an earlier break-up timing of 8 days which corresponds to the observed median variability of ± 8 days, the introduced excess energy due to a changing surface albedo from ice to water translates to melting 0.5 m thick ice at the melting point or heating up a water depth down to 35 m by 1 K across the entire surface area of each respective lake. Upscaling the results to 100486 lakes across the regions S, SW and NW which correspond to 64.5 % of all lakes or 62.1 % of the overall lake area in Greenland yields an estimate of 1.8 * 10^6 TJ additional energy input. This translates to melting 5.8 Gt ice at the melting point or warming 432.3 Gt water by 1 K.

1 Introduction

Lake ice plays an important role in biological, chemical, and physical processes of cold region freshwater (Duguay et al., 2015). Freshwater ice in the Arctic and its response to climate change have a variety of effects on hydrologic, ecological, and socio-economic systems (Prowse et al., 2011) while climate change being one of the most severe threats to global lake ecosystems (Woolway et al., 2020). The duration of lake ice controls the seasonal heat budget of lakes and may have an effect on both regional climate and weather events (Brown and Duguay, 2010; Duguay et al., 2015). The timings of lake ice freeze-up and break-up, i.e., lake ice phenology, are relevant climate indicators and can be useful for monitoring environmental changes (Adrian et al., 2009; WMO et al., 2023a). Therefore, lake ice is a parameter of the Essential Climate Variable (ECV) "lakes" and included in monitoring programs such as the World Meteorological Organization (WMO) Global Climate Observing System (GCOS) (WMO et al., 2023a) and the European Space Agency (ESA) Climate Change Initiative (CCI) (Climate Change Initiative Lakes, 2023). The scientific value of lake research and the important role of lakes for humans makes them incorporated in the United Nations' Sustainable Development Goals No. 6 (Clean Water and Sanitation) and

https://doi.org/10.5194/egusphere-2023-1762
Preprint. Discussion started: 2 August 2023

No. 13 (Climate Action) (United Nations, 2023), and an essential component of the United Nations Framework Convention on Climate Change (UNFCCC) and the Intergovernmental Panel on Climate Change (IPCC) (Woolway et al., 2020).

Lake ice freeze-up and break-up are results of energy surplus or deficit in the energy balance of the lake. The energy exchanges between the ice cover or water surface and the atmosphere are mainly determined by air temperature, precipitation, wind and radiation. The seasonal changes in solar radiation, however, are the main influence for the overall energy availability to form and decay lake ice cover (Brown and Duguay, 2010). Both linear and non-linear relation between lake ice break-up timing and air temperature have been established, while stronger correlations with latitude were identified compared to elevation (Weyhenmeyer et al., 2004; Williams et al., 2004; Williams and Stefan, 2006; Jeffries et al., 2012).

Satellite remote sensing provides the necessary means to increase the spatial coverage and temporal frequency of ground-based observations of lake ice phenology which have been globally declining since the 1980s (Duguay et al., 2015). Synthetic aperture radar (SAR) backscatter exhibits differences between water and ice due to dielectric properties of the materials (Unterschultz et al., 2009) and therefore allows for identifying the phenological state of the lake ice cover. Several studies investigated the evolution, characteristics and phenology of freshwater ice such as river ice (e.g., Lindenschmidt et al., 2011; Stonevicius et al., 2022) and lake ice (e.g., Wang et al., 2018; Murfitt and Duguay, 2020; Tom et al., 2020; Siles et al., 2022) from radar imagery, while we are not aware of a comprehensive study on lake ice break-up timing across Greenland.

In this study, we explore the potential of utilizing Sentinel-1 (S1) synthetic aperture radar (SAR) data for identifying temporal and spatial variations of lake ice break-up across S, SW and NW Greenland between 2017 and 2021 and assess its latitudinal and vertical gradients. Peripheral lakes in Greenland, i.e., lakes excluding supra- and proglacial lakes, make up for approximately 0.7 % of the overall land area or approximately 3 % of the unglaciated area. Therefore, we aim to quantify the additional energy input by estimating excess radiation and energy for a potential earlier lake ice break-up timing from the observed lake ice break-up variabilities.

1.1 Background and Related Studies Using SAR for Studying Lake Ice Cover

The transmitted pulse of SAR systems interacts with the Earth surface and only a portion of it is backscattered to the receiving antenna. The amplitude and phase of the backscattered signal depends on the physical (i.e., geometry, roughness) and electrical properties (i.e., permittivity) of the imaged object (Moreira et al., 2013). The reflection, transmission, and absorption of the radar beam at lake ice is governed by the (combination of) interactions with water, ice, snow and air. The differences in the amplitude of the backscattered signal between ice and water due to the influence of the electrical properties (Unterschultz et al., 2009) can be utilized to identify the phenological state of the ice cover of lakes.

Using satellite data for studying lake ice possesses several advantages over ground observations in terms of data availability and accessibility. Ground observations of lake ice may be limited due to access to remote and unpopulated areas, safety hazards during freeze-up and break-up periods. Satellite observations are independent from these restrictions and offer a relatively rapid, lower-cost and spatially broader way of obtaining data (Siles et al., 2022). Radar is independent from daylight and weather conditions, and S1 SAR data is available and accessible at high spatial and temporal resolutions (Sentinel-1 SAR User

https://doi.org/10.5194/egusphere-2023-1762
Preprint. Discussion started: 2 August 2023

Guide, 2023). While still being dependent on field measurements for validation, lake ice studies from remote sensing are no longer dependent solely on a small number of ground observations but can produce results and extrapolate measurements across landscapes and regions (Murfitt and Duguay, 2021).

Wang et al. (2018) utilized dual polarized RADARSAT-2 imagery for a semi-automated, pixel-by-pixel ice/water classification at Lake Erie and provided an overall accuracy of up to 90.4 %. Using a deep learning network, Tom et al. (2020) conducted a pixel-based lake ice phenology classification from S1 SAR data for three alpine lakes in Switzerland and found accuracies well above 90 %. They demonstrated that the phenological state of the lake ice cover of non-transition days (i.e., ice/snow or water) can be identified confidently. Murfitt and Duguay (2020) utilized S1 high-density time series data to monitor ice phenology of the High Arctic Lake Hazen (Canada) and demonstrated mean errors between 3 and 7 days for identifying the timing of lake ice break-up. Since it has been demonstrated that lake ice phenology can be assessed using SAR data, we developed a dynamic numerical threshold to automatically identify the lake ice break-up timing from SAR backscatter across Greenland.

2 Data

2.1 Greenland Lake Inventory

The Greenland lake inventory (Styrelsen for Dataforsyning og Infrastruktur, 2023) includes 155870 peripheral lakes in Greenland ranging from 1.6 * 10^{-3} km^2 to 138 km^2. The vector data set is part of the data inventory Databoks Grønland (2023) and based on commercial satellite images with a resolution of 0.5 m primarily from summer months in the period from 2017 to 2021.

2.2 Sentinel-1 SAR

The Sentinel-1 mission consists of satellites S1A and S1B which acquire C-band SAR data with a centre frequency of 5.407 GHz (Sentinel-1, 2023). Single polarized horizontal transmit/horizontal receive (HH) Level-1 ground range detected (GRD) data in both ascending and descending orbit acquired in Interferometric Wide (IW) swath mode with a swath width of 250 km is used in this study (Sentinel-1 SAR User Guide, 2023). The HH polarization and IW swath mode are chosen due to the comprehensive spatial coverage of Greenland. The satellites have near-polar, sun-synchronous orbit with a 12-day repeat cycle and 175 orbits per cycle for each satellite. S1A and S1B have the same orbit plane with a 180° orbital phasing difference which results in an actual repeat cycle of 6 days with both satellites operating (Sentinel-1 SAR User Guide, 2023). For determining the timing of lake ice break-up, it is crucial to utilize the highest possible temporal resolution of the SAR data, which is why we use data from both ascending and descending orbits. The combination of both orbital modes and the high overlap of the acquisitions due to converging orbits close to polar regions leads to a coverage with a revisit frequency of below 2 days for most of Greenland (Sentinel-1 SAR User, Guide 2023). The prerequisite of both satellites being operational to ensure this revisit frequency constrains our study period to 2017-2021.

https://doi.org/10.5194/egusphere-2023-1762
Preprint. Discussion started: 2 August 2023

We use the Earth Engine Code Editor (2023) and load SAR data from the Earth Engine Data Catalogue (2023) which allows for performing an online analysis of large datasets with virtually no computational cost on a desktop computer. Accessing the data as Level-1 GRD product means that border noise removal, thermal noise removal, radiometric calibration and terrain correction have already been performed following The Sentinel-1 Toolbox (2023) pre-processing steps leading to a calibrated and ortho-rectified product with a pixel size of 10 x 10 m. The ground range detection process projects the slant range coordinates of the radar data represented by range and azimuth onto the ellipsoid of the Earth resulting in a product which has approximately square spatial resolution and square pixel spacing (Sentinel-1 SAR Technical Guide, 2023). Border noise removal deals with low intensity noise and invalid data on scene edges. The thermal noise correction removes additive noise in sub-swaths to help reduce discontinuities between sub-swaths for scenes in multi-swath acquisition modes (Sentinel-1 Algorithms, 2023). Radiometric calibration ensures that the intensity value represents the value of the reflectivity, i.e., the radar cross section normalized to area (Moreira et al., 2013). This backscatter coefficient σ_0 can vary by several orders of magnitude and is therefore converted to decibel, as shown in Eq. (1).

$$\sigma_0 = 10 \log_{10} \sigma_{0\,raw} \quad (1)$$

It measures whether the radiated terrain scatters the incident microwave radiation preferentially away from the SAR sensor ($\sigma_0 < 0$) or towards the SAR sensor ($\sigma_0 > 0$) (Sentinel-1 Algorithms, 2023). Terrain correction ensures that the location of any pixel in the SAR image is directly associated to the position on the ground. Radar only measures the projection of a three-dimensional scene on the radar coordinates slant-range and azimuth. This causes effects such as shadow for areas hidden from the radar illumination as well as foreshortening and layover manifested by a stretch and compression of sloped terrain (Moreira et al., 2013). The terrain correction (or ortho-rectification) is based on the ASTER Global Digital Elevation Model (GDEM) (U.S./Japan ASTER Science Team, 2023) given the high-latitude location of the study area (> 60° N) (Sentinel-1 Algorithms, 2023).

2.3 Incoming Shortwave Radiation and Air Temperature

For estimating excess radiation and energy due to variability in the break-up timing and investigating potential correlations with air temperature, we acquired incoming shortwave radiation and air temperature at 2 m data as climatological daily mean values for the period 1991-2020 from RACMO2 (Noël et al., 2018). The four nearest grid points of the model from the coordinates of each respective lake centre point were selected in order to approximate the radiation and temperature data using Delaunay triangulation (Delaunay, 1934) with cubic interpolation.

https://doi.org/10.5194/egusphere-2023-1762
Preprint. Discussion started: 2 August 2023

3 Methods

3.1 Pre-Processing Lake Inventory and SAR Data

We retrieved SAR backscatter data of 14336 lakes which have a surface area ≥ 0.1 km^2 to exclude potential inaccuracies due to the lake size. Time series of lakes with a temporal resolution below 2 days are excluded from the analysis to produce robust results. While the acquisition frequency varies spatially and might be as high as 1 day, we assume a maximum temporal resolution of 2 days for the entire dataset which falls short of meeting the daily acquisition criteria of the GCOS ECV lake ice cover for climate monitoring (WMO et al., 2023b). Backscatter data which lacks a pronounced annual evolution and exhibits strong uniformal characteristics are also excluded. This means that only lakes with a difference of ≥ 8 dB in mean values of σ_0 between January/February (i.e., most certainly ice covered) and August/September (i.e., most certainly ice free) are considered.

3.2 Detecting Lake Ice Break-up from SAR Backscatter

The term "lake ice break-up" used in this study describes the timing, i.e., day of year (DOY), when most of the lake surface is liquid water and is therefore an approximation to the timing of "water clear of ice" (WCI) (WMO et al., 2023b). Once snowmelt starts on lake ice, water collects around the margins where it warms as it absorbs solar radiation and accelerates melting due to positive feedback (Jeffries et al., 2012). We assume that lake ice is longest present in the central areas of the lake and therefore aim to detect the presence or absence of ice in the central 20 % of the lake surface area which means that the σ_0 values are averaged for this central portion. This results in an area of approximately 0.02 km^2 for the smallest lake, which corresponds to at least 200 pixels considered for averaging.

We apply a locally weighted scatterplot smoothing (LOWESS) filter to attenuate the temporal variability of σ_0 caused by varying incidence angles due to both ascending and descending orbits to ensure a more robust and confident ice break-up detection (Fig. 1a). We found the choice of 1 % of the data for LOWESS filtering to provide robust results for the analysis. For each lake, a dynamic numerical threshold is applied in each year to identify the timing of ice break-up. This yearly threshold amounts to 25 % of the σ_0 difference between the 98th and 2nd quantile and must be at least 2.5 dB. The timing of lake ice break-up is detected when the absolute value of σ_0 decrease exceeds the threshold value within three consecutive acquisitions. Once the break-up timing is identified from the LOWESS data, the day of year (DOY) of lake ice break-up is assigned to the lowest σ_0 value of the raw backscatter signal within five acquisitions ahead of the detected drop in the LOWESS data (Fig. 1a). The detection algorithm is applied for the period starting from 1 May to exclude early misdetections.

https://doi.org/10.5194/egusphere-2023-1762
Preprint. Discussion started: 2 August 2023

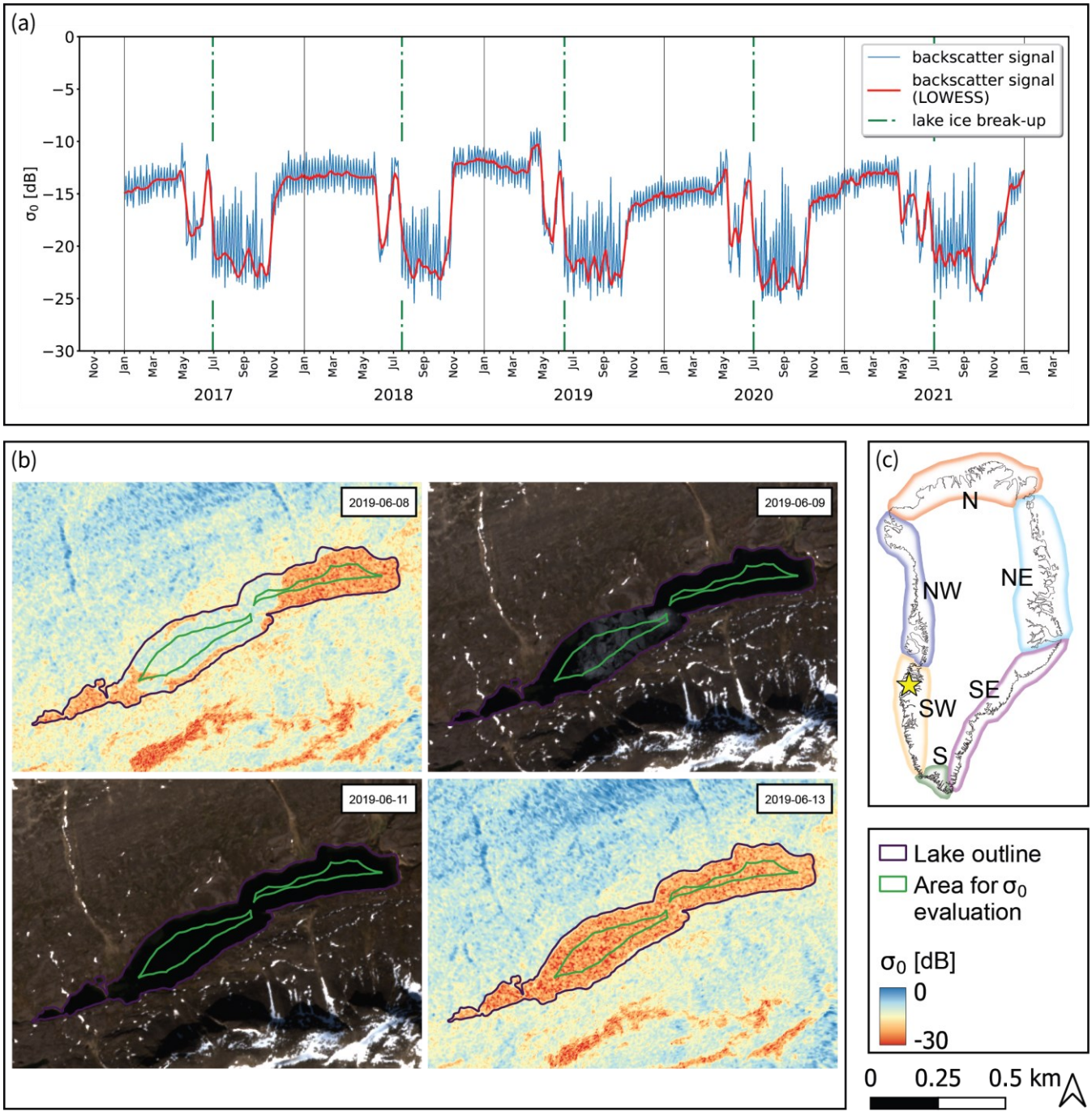

Figure 1: (a) Sentinel-1 (S1) synthetic aperture radar (SAR) backscatter (σ_0) and lake ice break-up timings for lake 28300 detected from a dynamic numerical threshold assessing the σ_0 decline from being ice covered to open water. While the LOWESS smoothed backscatter is utilized to confidently identify the period of break-up, the actual break-up timing is derived from the raw backscatter signal. The σ_0 decline and recovery just before the apparent lake ice break-up indicates the onset of snow and ice melt. (b) S1 and Sentinel-2 (S2) images of lake 28300 during break-up in 2019. The S2 scene shows water clear of ice (WCI) on 11 June 2019, while the break-up timing from S1 is detected on 13 June 2019. (c) Regions of Greenland for the spatio-temporal analysis.

https://doi.org/10.5194/egusphere-2023-1762
Preprint. Discussion started: 2 August 2023

Figure 1a shows a typical SAR backscatter evolution for the period 2017 to 2021 with detected break-up timings. High σ_0 values (e.g., Nov-May) are governed by surface dry conditions of snow and ice (Unterschultz et al., 2009). The first major declines of σ_0 in a given year (e.g., May-Jun) indicates the onset of melt processes at the surface of the lake ice cover. A smooth, wet ice surface decreases the amount of backscatter due to specular reflection of the radar beam in a direction away from the sensor A rough, wet ice surface increases the amount of backscatter due to diffuse scattering, reflecting the radar beam nearly uniformly in all directions and directing a proportion of the incident energy back toward the sensor (Unterschultz et al., 2009). The progressing melt on the lake surface leading to a rougher, wetter surface explains the σ_0 recovery before the major backscatter decline in summer indicating lake ice break-up. Figure 1a shows that in several years (e.g., from 2017 to 2020), the evolution of σ_0 might be clearly pronounced, while in other years (e.g., 2021) the backscatter decline and identification of the break-up timing is more complex. This is due to the nature of break-up processes being more complex due to melting on top and bottom (Jeffries et al., 2012) or varying acquisition conditions.

Figure 1b shows the results of lake 28300 in SW Greenland to demonstrate the detection of lake ice break-up in 2019 from SAR data compared to optical satellite imagery from the Sentinel-2 (S2) mission. The detection algorithm identifies the lake ice break-up timing on 13 June 2019 from S1 backscatter data, while the S2 image shows water clear of ice on 11 June 2019 which can be taken as the accuracy of the method.

3.3 Analysing Spatial Patterns of Lake Ice Break-Up Timing

The study area is divided into six regions (N, NE, SE, S, SW, NW) to explore spatio-temporal statistics (Fig. 1c). We chose a confidence level of 0.95 to assess significant differences between regions and years, respectively. Furthermore, we grouped lakes into sections of 1° N latitude and 100 m elevation, respectively, to assess spatial gradients in greater detail. In the result statistics we include only lakes with detected ice break-up timings in every given year (2017-2021) to get robust detection statistics and to mitigate random detections. Furthermore, we manually removed obvious misdetections after visual inspection of the backscatter time series since we prioritize robust results statistics over a fully-automatically detected larger sample size that includes misdetections.

3.4 Assessing Climatological Variables in terms of Lake Ice Break-Up Timing

3.4.1 Calculating Cumulative Positive Degree Days

In order to understand the relationship between the annual evolution of air temperature, incoming radiation and median lake ice break-up timings we calculated the climatological mean of positive degree days (PDDs) from RACMO2 2 m daily air temperature averages for the period 1991 to 2020 and analysed them as cumulative values from 1 January until the median DOY of break-up.

https://doi.org/10.5194/egusphere-2023-1762
Preprint. Discussion started: 2 August 2023

3.4.2 Calculating Excess Radiation and Energy

In order to determine the impact of varying lake ice cover on the radiation and hence the energy balance, we acknowledge several factors: (I) The surface albedo of the lake surface changes rather abruptly from ice to open water. That way, the same radiation and energy input gets converted to drastically higher energy amounts at the surface after ice break-up. (II) Depending at what time of the year the break-up happens, one will have a different impact on the energy balance. To illustrate the different impact a given change in lake ice break-up may have, we assume three arbitrary lakes of the same size at the same latitude (and hence with the same arbitrary potential incoming shortwave radiation values) and show the impact in a conceptual way in Fig. 2. Assume that, for instance due to elevation differences, lake A typically breaks up some weeks before, B at the time of incoming radiation maximum, and C some weeks after. If we now assume changing conditions in a way that all three lakes break up 8 days (which corresponds to the median MAD and is described in Eq. (4)) earlier than under 'regular' conditions, we see the following: For case A, less energy gets added, since it is at a time when radiation input is comparably low, while B changes the energy input more strongly. For C it means that despite the same temporal lag to the radiation maximum compared to A, the excess radiation and energy input gets higher since the period falls into a time with high incoming radiation. We coin the terms "excess radiation (input)" and "excess energy (input)" to describe the additional added radiation and energy due to an earlier lake ice break-up timing of 8 days compared to the observed median timings between 2017 and 2021 for each respective lake. (III) The lake size plays a role for total budget considerations: Large lakes have larger surface areas over which the energy can be accumulated. (IV) Finally, the shortwave radiation input is determined by latitude and altered by regional effects (e.g., cloud cover) or local effects (e.g., shading due to geometry).

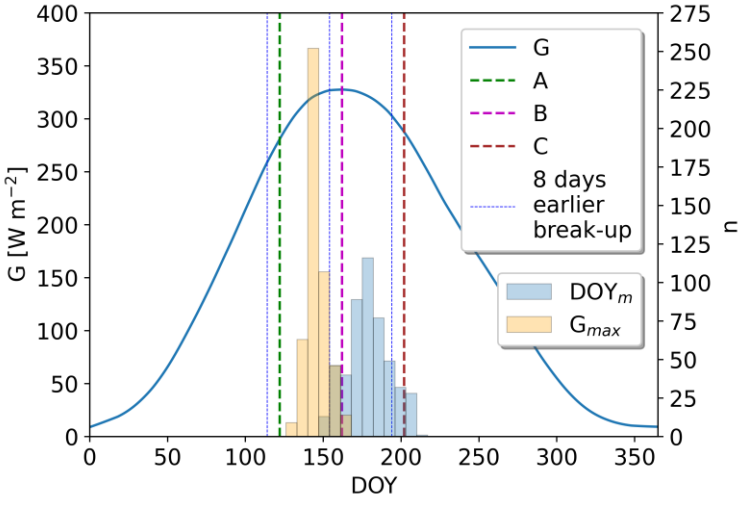

Figure 2: Conceptual lake ice break-up timings of three arbitrary lakes A, B, C and histograms of lake-specific median lake ice break-up DOY_m and timing of maximum incoming radiation G_{max}. Assuming that all three lakes break up a fixed period earlier than their median break-up timings (in this case 8 days earlier which is the median variability in our data), it can be hypothesized that considering the annual evolution of global radiation G at the surface, lake A receives less additional energy, lake B at the solar radiation maximum the most, and lake C comparably higher additional energy than lake A. Median day of year (DOY) of DOY_m and G_{max} in our data are 178 and 145, respectively, indicating that most of the lakes will correspond to lake B.

https://doi.org/10.5194/egusphere-2023-1762
Preprint. Discussion started: 2 August 2023

We quantify the excess radiation input H_{SW} [J m^{-2}] for each lake as a consequence of an earlier break-up by integrating the shortwave radiation balance (incoming radiation G [W m^{-2}] minus the reflected shortwave incoming radiation R [W m^{-2}]) between 8 days before DOY_m and the median lake ice break-up timing DOY_m, as shown in Eq. (2).

$$H_{SW} = \int_{DOY_m - MAD}^{DOY_m} G(t) - R(t)\, dt \quad (2)$$

The reflected shortwave incoming radiation R [W m^{-2}] is calculated from the albedo difference $\Delta\alpha$ between the assumed values of lake ice α_i (0.9) and open water α_w (0.1), as shown in Eq. (3)

$$R = G\,\Delta\alpha \qquad with \qquad \Delta\alpha = \alpha_i - \alpha_w = 0.8 \quad (3)$$

The chosen 8 days for the hypothesized earlier lake ice break-up correspond to the median of the lake-specific median absolute deviation MAD describing the variability of the annual break-up timings DOY_i around the median DOY_m of this period, as shown in Eq. (4),

$$MAD = median(|DOY_i - DOY_m|) \qquad with \qquad DOY_m = median(DOY_i) \quad (4)$$

where DOY_i stands for the break-up timing in each respective year from 2017 to 2021. This can be regarded as a realistic period for an assumed earlier deviation of the break-up timings of all lakes to assess the impact of varying lake ice cover on the radiation balance.

Furthermore, we calculate the excess energy input E_{SW} [J] for each lake by multiplying the excess radiation H_{SW} [J m^{-2}] for the 8-days-earlier lake ice break-up with the respective lake areas A_i [m^2], as shown in Eq. (5).

$$E_{SW} = H_{SW}\, A_i \quad (5)$$

That way, we consider general radiation conditions, lake size and albedo change and express its reaction on a change in timing. Clearly, a change of the break-up timing at or just after the radiation maximum of a large lake will have a higher impact than a change later in the season for a small lake.

In order to make the results more tangible, we calculate what the excess energy inputs E_{SW} mean in terms of mass and volume ice melt at the melting point (m_i, V_i) and water temperature increase (m_w, V_w). For this we convert the summed energy input E_{SW} of all lakes using the latent heat of fusion L_f (334000 J kg^{-1}), the specific heat capacity of water c_w (4184 J kg^{-1}K^{-1}) and assumed densities of ice at the melting point ρ_i (999 kg m^{-3}) and water close to freezing point ρ_w (999 kg m^{-3}), as shown in Eq. (6) and Eq. (7).

$$m_i = \frac{\Sigma E_{SW}}{L_f} \qquad and \qquad V_i = \frac{m_i}{\rho_i} \quad (6)$$

$$m_w = \frac{\Sigma E_{SW}}{c_w} \qquad and \qquad V_w = \frac{m_w}{\rho_w} \quad (7)$$

https://doi.org/10.5194/egusphere-2023-1762
Preprint. Discussion started: 2 August 2023

3.5 Validating Detected Lake Ice Break-Up Timings

The break-up detection is assessed and validated in three ways: (I) We utilize daily time-lapse images of three lakes (Badesø, Langesø, Quassi-sø) in vicinity of Kobbefjord (SW Greenland) between 2017 and 2020 (Abermann et al., 2019) to quantify the mean error of lake ice break-up of those lakes compared to the detection algorithm. (II) We use lake ice break-up data from observations, thermistor data and satellite imagery in the Kangerlussuaq area (SW Greenland) between 2017 and 2021 (Saros et al., 2019). While there are no corresponding lakes from the validation data included in our study due to a lack of pronounced radiometric properties, we compare median lake ice break-up timings between 11 lakes used for validation and 14 lakes in our study in vicinity to each other. (III) We access daily data from ESA CCI (Climate Change Initiative Lakes, 2023) for "lake ice cover (LIC)" to validate the break-up timing of two lakes (SW Greenland). This data is generated from MODIS imagery from both the Terra and Aqua satellite missions.

4 Results

4.1 Lakes and Regions Suitable for Lake Ice Break-Up Detection and Analysis

We restrict our analyses to the sectors S, SW, and NW since a comprehensive analysis for lakes in N, NE and SE is not possible due to challenging radiometric characteristics and/or temporal resolution (Table A1, Table A2), leaving a too small sample size. Since we only consider lakes with detected break-up timings in every given year between 2017 and 2021 and remove obvious outliers manually, we end up analyzing 563 lakes, which are 21 lakes in S, 450 lakes in SW and 92 lakes in NW. This corresponds to 0.4 % of all lakes or 6.8 % of the overall lake area in the inventory. Tha data coverage of RACMO2, however, allows for analyzing 491 lakes, which are 21 lakes in S, 406 lakes in SW and 64 lakes in NW regarding excess radiation and energy inputs and cumulative PDDs. This represents 0.3 % of all lakes or 6.8 % of the overall lake area in the inventory (Table A1, Table A2).

4.2 Lake Ice Break-Up Detection Validation

The detection of the lake ice break-up timings from SAR data proves to be conservative (i.e., later) compared to the lakes from all three validation approaches and allows characterizing break-up timing with a mean error of maximum 5 days. Yearly mean errors of the three compared lakes validated from time-lapse cameras range from 1-18 days exhibiting an overall mean error of 5 days (Table A3). Yearly differences between the median break-up timings of 14 lakes compared to 11 surrounding lakes used for validation in the Kangerlussuaq area range from 3-7 days with an overall difference of 5 days, indicating that the interannual variability is well captured (Table A4). The two lakes validated from the ESA CCI data yield yearly mean errors ranging from 0-5 days with an overall mean error of 2 days (Table A5).

https://doi.org/10.5194/egusphere-2023-1762
Preprint. Discussion started: 2 August 2023

4.3 Lake Ice Break-up Timing across S, SW, NW Greenland and Elevation Gradients

Median break-up DOYs of all lakes range between 159 in 2019 and 191 in 2018, which corresponds to dates between 8 June and 10 July (Fig. 3). Regional annual median DOYs range between 168 and 212 (S), 159 and 191 (SW), and 153 and 188 (NW). Annual lake ice break-up DOYs in S are significantly later for 2018 to 2021 compared to SW and NW. In 2017, the median break-up DOY in S exhibits no difference to SW and is significantly earlier compared to NW. The annual break-up timings in SW are significantly earlier in 2017 and significantly later in 2021 compared to NW.

Lake-specific break-up timings as well as median break-up DOYs for 2017 to 2021 increase with elevation (Fig. 4a), while no confident latitudinal gradients nor correlations with lake surface area could be identified (Fig. 4b). Median break-up DOYs for the period 2017 to 2021 increase by 3 DOY per 100 m elevation gain ($r = 0.76$) (Fig. 4a), while yearly lake ice break-up DOYs show strong correlations ($0.51 \leq r \leq 0.78$) with elevation exhibiting increases of 2-4 DOY per 100 m (Fig. C1). For a given elevation band, we find that lake ice in more northern latitudes tends to break-up later but exhibiting only weak correlations.

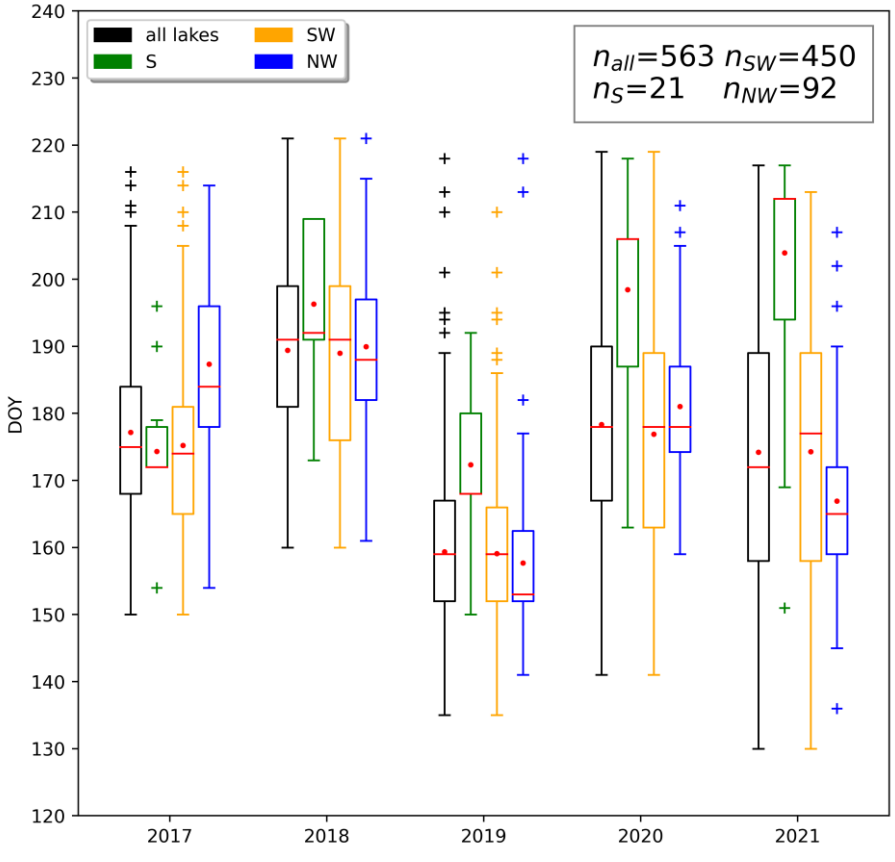

Figure 3: Lake ice break-up timings of all studied lakes and grouped by region. Red lines indicate median values, while red dots represent mean values. Median break-up timings are earliest in 2019 (8 June) and latest in 2018 (20 July). Lakes in the region S break up significantly later in 2018-2021 compared to the other regions, while lakes in NW tend to break up earliest. This can be attributed to mainly higher elevated lakes in S and mainly lakes close to sea level in NW.

https://doi.org/10.5194/egusphere-2023-1762
Preprint. Discussion started: 2 August 2023

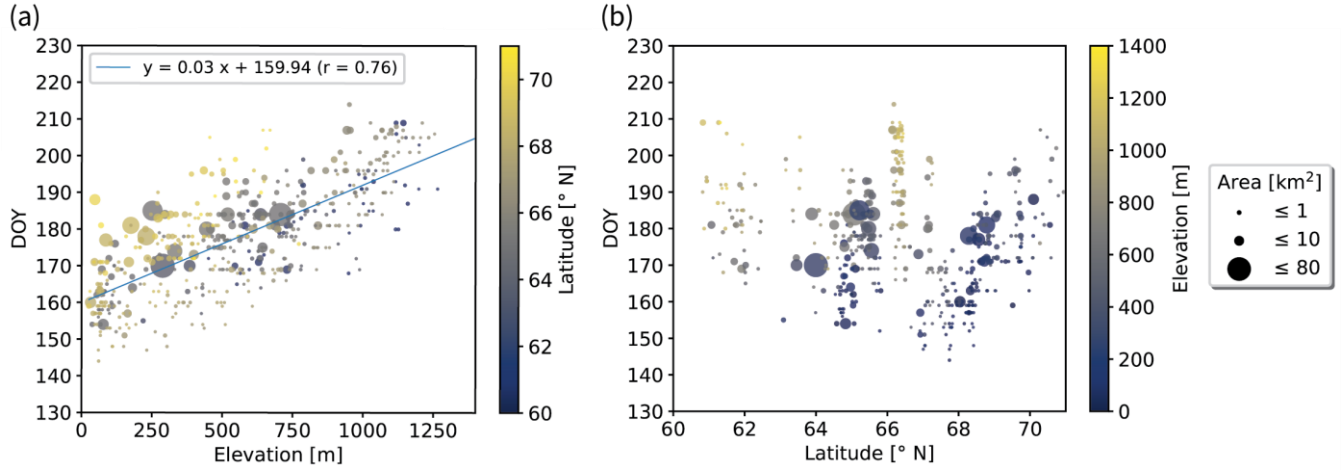

Figure 4: Median break-up timings DOY_m for the period 2017 to 2021 vs (a) elevation and (b) latitude. DOY_m increase by 3 DOY per 100 m elevation gain exhibiting a strong correlation (r = 0.76). Only a weak correlation with latitude can be identified when grouping lakes of similar elevation, we there is no relationship between break-up timing and lake size.

Subdivided into latitudinal bands of 1° between 60° N and 71° N, strong correlations (up to r = 0.89) between break-up timing and elevation can be identified in several years. Those exhibit an increase of 3-6 DOY per 100 m depending on the latitudinal band and the elevation range (Fig. C2-Fig. C5). The median break-up dates for the period 2017 to 2021, except between 60-61° N and 70-71° N, show strong correlations ($0.64 \leq r \leq 0.85$) increasing by 3-6 DOY per 100 m elevation increase.

4.4 Lake Ice Break-up Timing compared to cumulative PDDs until Lake Ice Break-Up

Figure 5 shows an increase of cumulative PDDs until lake ice break-up with increasing median break-up DOYs. A later break-up timing at lower latitudes can be observed in Fig. 5a when comparing lakes in a similar cumulative PDD range. Figure 5b shows that lakes with similar cumulative PDDs experience a later lake ice break-up at higher elevation. This is due to mainly higher elevated lakes at lower latitudes as opposed to lower elevated lakes at higher latitudes. Comparing two lakes at different elevation with a similar break-up timing, we see that a higher elevated lake with lower cumulative PDD values needs a comparingly higher energy input (or less energy output) to accommodate for the same break-up timing as the lower elevated lake with comparingly higher cumulative PDDs. This is provided by a location at lower latitudes with comparingly more incoming shortwave radiation.

https://doi.org/10.5194/egusphere-2023-1762
Preprint. Discussion started: 2 August 2023

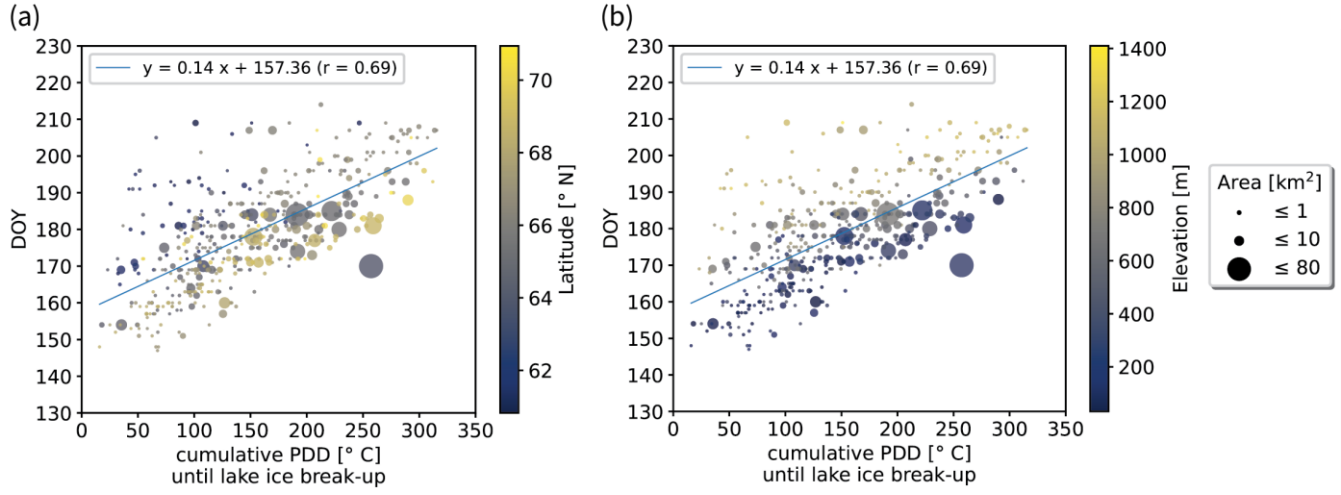

Figure 5: Median break-up timings DOY_m for the period 2017 to 2021 vs cumulative positive degree days (PDD) until lake ice break-up with colour signatures for (a) latitude and (b) elevation. The influence of air temperature and radiation on the break-up timing (i.e., in the energy budget) can be assessed when comparing two lakes at different elevation with a similar break-up timing. While the lower elevated lake has higher cumulative PDD values and is located at higher latitude, the higher elevated lake with lower cumulative PDDs is located more south.

4.5 Excess Radiation and Energy from earlier Lake Ice Break-Up

Referring to the concept shown in Fig. 2 which describes the median lake ice break-up timings in relation to the timing of maximum incoming solar radiation, we find that virtually no lakes represent case A (< 0.01 %), approximately 5 % represent case B which are around the respective radiation maximum (± 8 days), while case C applies to approximately 95 %. The median time difference between the lake-specific maximum incoming radiation and median break-up amounts to 35 days (Fig. D1). Figure D1 shows that excess radiation H_{SW} is highest for lakes around and after the radiation maximum, while H_{SW} values are decreasing with increasing later timing of the median break-up (i.e., increasing distance from the solar radiation maximum).

Highest H_{SW} values can be found at low latitudes as well as high-latitude lakes at lower elevation (Fig. 6). At lakes with similar latitude, higher H_{SW} values are found at lower elevations, while at lakes with similar elevation, excess radiation values are typically higher at lower latitude.

https://doi.org/10.5194/egusphere-2023-1762
Preprint. Discussion started: 2 August 2023

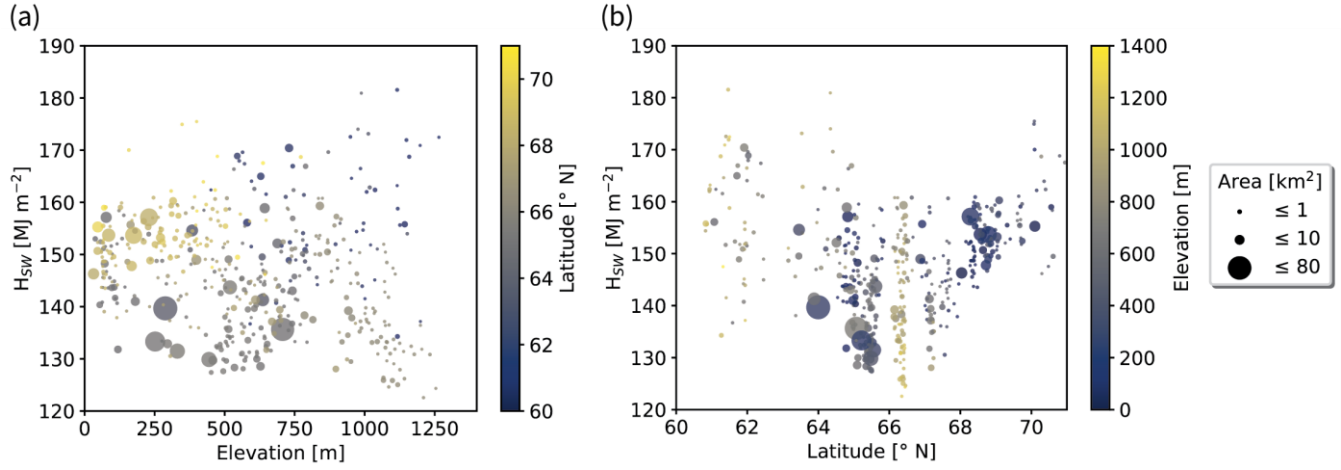

Figure 6: Excess radiation H_{SW} due to lake-specific break-up timings which are 8 days earlier compared to the median break-up timings for the period 2017 to 2021 vs (a) elevation and (b) latitude. High H_{SW} values are found for lakes at low latitudes as well as at high latitudes with low elevation.

Figure 7 shows the lake specific results for E_{SW} as a function of latitude (Fig. 7a) and elevation (Fig. 7b). We clearly find larger E_{SW} values for larger lakes and a weaker, yet visible dependence with latitude. Regarding a relation to elevation, we see generally larger E_{SW} for lower elevations, which is partly due to the fact that larger lakes typically develop in lower elevations. Also, the fact that high-elevated lakes typically break up later after the radiation maximum plays a role in that regard. We find that the summed excess energy of all 491 analyzed lakes which amounts to 133250 TJ corresponds to melting 0.4 Gt ice or an ice cube of 7.4 km length. Likewise, the same energy input could heat up 31.9 Gt water or a water cube of 31.7 km length by 1 K.

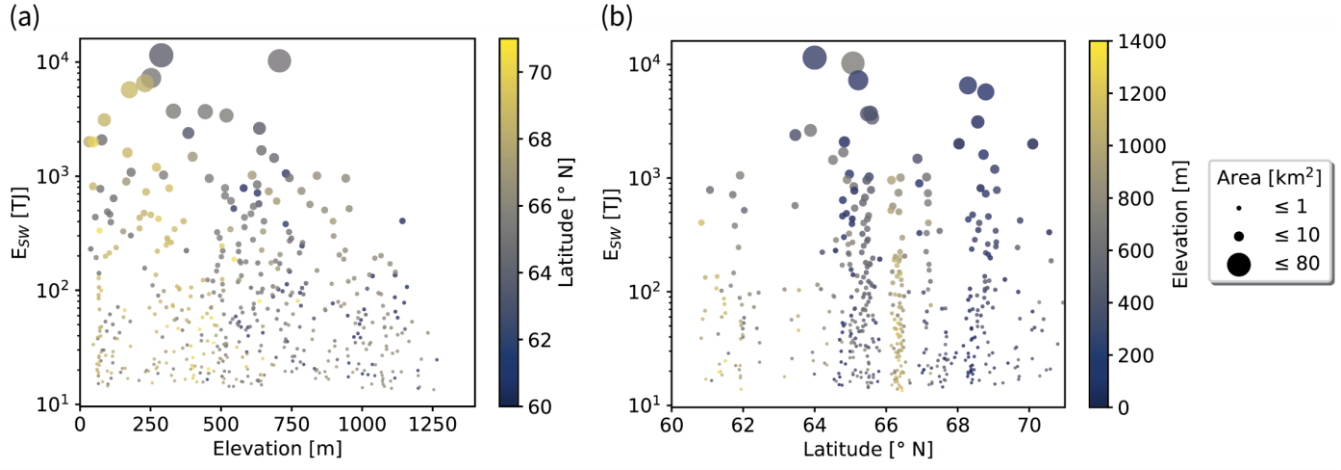

Figure 7: Excess energy E_{SW} due to lake-specific break-up timings which are 8 days earlier compared to the median break-up timings for the period 2017 to 2021 vs (a) elevation and (b) latitude. Lake surface area strongly determines the excess energy. Largest E_{SW} are found at mid-latitudes and low elevation, since larger lakes typically developed there.

https://doi.org/10.5194/egusphere-2023-1762
Preprint. Discussion started: 2 August 2023

Our calculations on excess energy show that lake surface area strongly determines the added energy and explains more than 99 % of its variability in the dataset (Fig. D2). Referring the added energy in terms of ice melt and water temperature rise to the lake-specific areas in a simplified way which ignores lake bathymetry, we find that the excess energy input averagely corresponds to melting 0.5 m thick ice or heating up a water depth down to 35 m by 1 K across the entire surface areas. If we upscale our results to all 100486 lakes in S, SW and NW (< 71° N) Greenland based on the strong relationship between excess energy and surface area while assuming similar radiation conditions and lake ice break-up variabilities, we estimate an additional energy input of 1.8 * 10^6 TJ which corresponds to melting 5.8 Gt ice at the melting point or warming 432.3 Gt water by 1 K. This number of lakes corresponds to 64.5 % of all lakes or 62.1 % of the overall lake area in the inventory (Table A1, Table A2). To put this into perspective, the upscaled mass estimate of ice melt corresponds to approximately 30 to 60 % of the volume of Greenland peripheral glaciers published in recent studies (Hock et al., 2023).

5 Discussion

We assess that elevation more strongly determines lake ice break-up timing in Greenland than latitude does. For both all lakes and lakes grouped by latitudinal sections, we demonstrated that there are strong correlations between median break-up timings and elevation as well as yearly break-up timings and elevation. The significantly later timing of yearly median break-up DOYs in S compared to SW and NW in several years can be explained by the hypsometry of the terrain and the distribution of lakes with elevation (fewer lakes close to sea level). Local topography such as elevation and extent of fjord systems can have a strong influence on the timing of ice break-up. This is demonstrated by lakes with early break-up timings in close vicinity to fjords such as between 67.5° N and 68.5° N (Fig. 8a: orange arrow) as opposed to lakes with late break-up timings at high elevation areas (> 1000m) such as between 66.0° N and 66.5° N (Fig. 8a: blue arrow).

Williams et al. (2004) and Williams and Stefan (2006) assessed lake ice break-up timings of approximately 140 lakes in North America (between 40° N and 82.5° N) from records ranging from 1848 to 1997 and found that there is a strong relationship between break-up timing and latitude, arguing that geographic latitude is a good indicator of climate. They showed that only a week relationship between elevation and the timing of break-up was observed when grouping the data by region, presenting an increase of break-up timing of 2 days per 100 m elevation increase. In our study, however, we find strong correlations between break-up timing and elevation and only a weak relationship with latitude when grouped. This again highlights the influence of the distinctive spatial configuration of lakes in Greenland determined by the proximity to both the ocean and the Greenland Ice Sheet, the presence of fjord systems and the rapid elevation increase. We assume that local climates and consequently the lake ice break-up timings are greatly influenced by those parameters.

Lake ice break-up timings of the years 2018 (Fig. 8b) and 2019 (Fig. 8c) which exhibit the latest (DOY 191; 10 July) and earliest (DOY 159; 8 June) median lake ice break-up DOYs within the observed period are in line with temperature observations. Mean summer and July temperatures in 2019 were among the 6 warmest years (1981-2019), while comparably cooler JJA air temperatures at Greenland coastal stations were recorded in 2018 (Hanna et al., 2021).

https://doi.org/10.5194/egusphere-2023-1762
Preprint. Discussion started: 2 August 2023

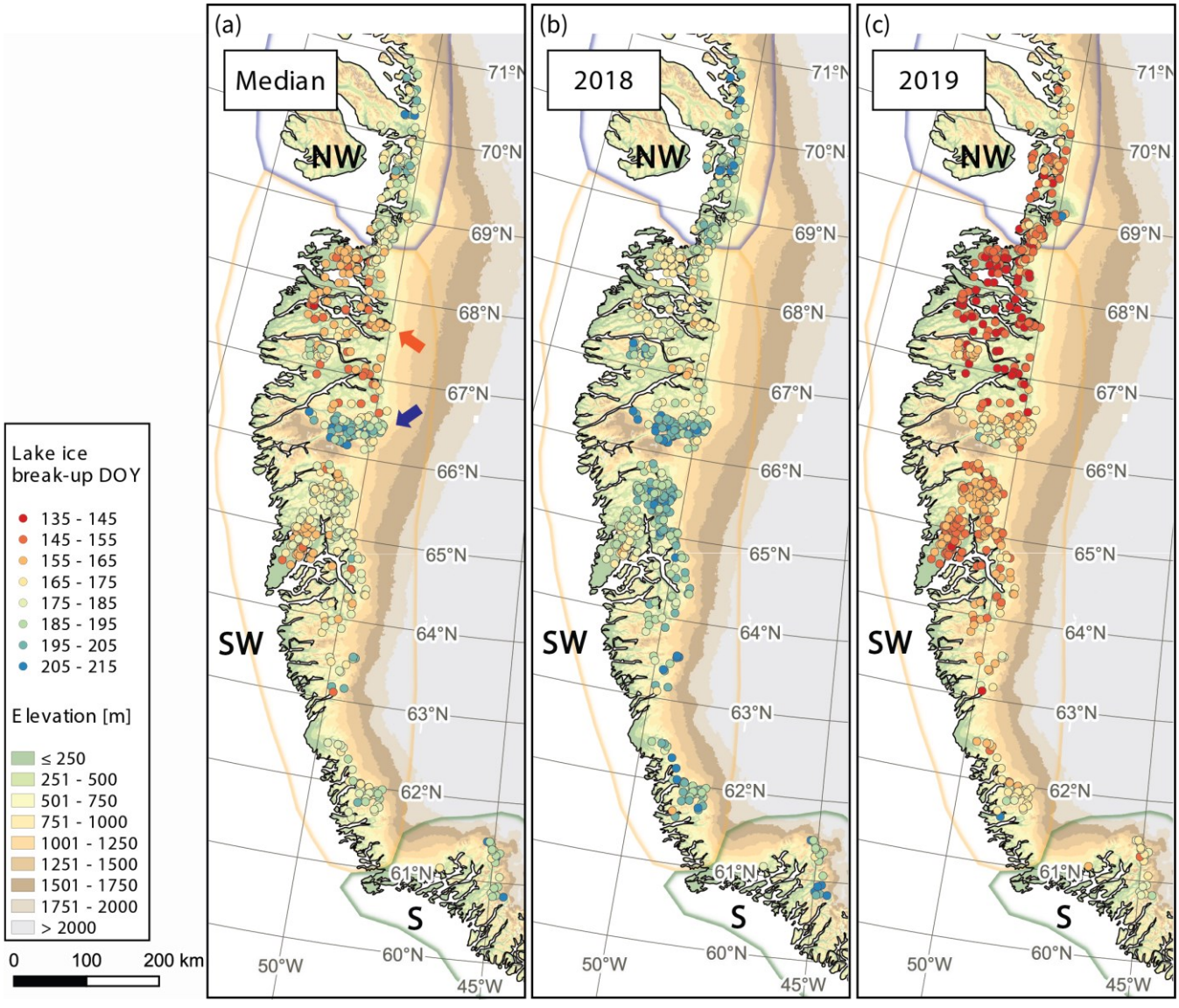

Figure 8: (a) Median lake-specific break-up timings for the period 2017 to 2021, and break-up timings for (b) 2018 and (c) 2019. Local topography such as higher elevation (blue arrow) and extent of fjord systems (orange arrow) can strongly influence lake ice break-up dates. The year 2018 exhibits the latest break-up timings while the year 2019 shows the earliest break-ups in our studied period, corresponding to median dates 10 July (DOY 191) and 8 June (DOY 159), respectively.

Our presented vertical gradients of break-up timings in the order of a few days must be interpreted in regards with temporal limitation of the data and method. The SAR data with an acquisition resolution of 2 days implies a maximum accuracy of ±1 day for detecting lake ice break-up, while the validation indicates that our automated detection exhibits a mean error of 2-5 days. Although our input data falls short of the GCOS ECV requirement of 1 day for climate monitoring from lake ice cover, we demonstrate a median break-up timing variability of 8 days and identify extreme years. The GCOS ECV requirements state that the temporal resolution of our study allows for contrasting extreme ice years, numerical weather forecasting and assessing

https://doi.org/10.5194/egusphere-2023-1762
Preprint. Discussion started: 2 August 2023

lake models (WMO et al., 2023b). In a related study, Murfitt and Duguay (2020) also utilized S1 high-density time series data to monitor ice phenology of Lake Hazen located in Nunavut, Canada (71.05° W, 81.78° N). They found mean errors of 3-7 days for comparing sectional WCI dates and 3-5 days for a pixel-based ice-off comparison, which is in agreement and in the order of our validation results.

Magnusson et al. (2000) found that lake ice break-up dates in the Northern Hemisphere from 1846 to 1995 became on average 6.5 days earlier, corresponding to an air temperature increase of approximately 1.2° C during this period. They claim that the interannual variability of break-up timings increased since 1950. Our observed variability of ± 8 days based on the period 2017-2021 lies above the observed break-up shift over 100 years, which might be either contributed to the increased variability in recent years, or due to the extreme years 2018 and 2019 greatly skewing the variability in the short observational period. The magnitudes of our estimated excess energies from earlier break-up timings indicate potential vast changes in the energy balance with increasingly earlier break-up dates and increasing variabilities due to a changing climate.

6 Conclusion

We demonstrated that temporal high-resolution S1 SAR data can be utilized to detect lake ice break-up timings in SE, S, SW and NW Greenland. Our presented lake ice break-up timing results prove to be robust and conservative (i.e., later) with a mean error of maximum 5 days and allow for a spatio-temporal characterization. We show that median lake ice break-up timings for the period 2017 to 2021 increase by 3 DOY per 100 m elevation increase, while no strong correlations can be found regarding latitude or lake area.

The 491 studied lakes exhibit a typical variability in break-up timing of ± 8 days. When we assume the break-up timing being 8 days earlier for each lake, the introduced excess energy corresponds to melting 0.5 m thick ice at the melting point or heating up a water depth down to 35 m by 1 K across the respective surface areas. Scaling up our results to 100486 lakes across S, SW and NW Greenland, the excess energy input amounts to approximately $1.8 * 10^6$ TJ for the hypothesized earlier lake ice break-up.

Excluding data from days with high wind speeds or coupling the SAR-based detection with optical detections from satellite systems (e.g., S2) might yield more robust results with a higher accuracy but might also additionally decrease the temporal resolution. Applying machine learning or deep learning algorithms as a next step might further improve the break-up detection and increase sample size. There is potential for exploring the relationship between break-up timing and climatological variables and assess the impact on the energy budget in greater detail by incorporating a variety of parameters into more complex models. Coupling satellite-derived break-up results with a greater number of ground observations and in-situ measurements of meteorological variables might further improve remotely sensed break-up detections. A continued study of lake ice break-up timings detected from spatial and temporal high-resolution SAR data such as from S1 will be of high importance in terms of climate monitoring with more data available from increasing operational periods. We aim at applying our algorithm for an analysis of lake ice break-up timing on a global scale.

https://doi.org/10.5194/egusphere-2023-1762
Preprint. Discussion started: 2 August 2023

Code/Data availability

Code and data is preliminarily and not publicly available under following link: https://unigraz-my.sharepoint.com/:f:/g/personal/christoph_posch_edu_uni-graz_at/EkW-sXE9S_5FrdnOFBlLT20Bxf3UpzphXUmVglDCpRgFaQ?e=RuGZad.

Author contribution

Christoph developed the detection algorithm, processed the data, and produced all results and plots. Jakob developed the idea and greatly determined the scope and direction of the study and displayed results. Tiago was involved and contributed the RACMO2 data to the study.

Competing interests

The authors declare that they have no conflict of interest.

Acknowledgements

We thank Václava Hazuková and Jasmine Saros for providing observations on lake ice break-up dates for lakes in the Kangerlussuaq area (SW Greenland). Their data greatly contributed to validating our detection algorithm.

References

Abermann, J., Eckerstorfer, M., Malnes, E., and Hansen, B. U.: A large wet snow avalanche cycle in West Greenland quantified using remote sensing and in situ observations. Natural Hazards, 97, 517–534, https://doi.org/10.1007/s11069-019-03655-8, 2019.

Adrian, R., O'Reilly, C. M., Zagarese, H., Baines, S. B., Hessen, D. O., Keller, W., Livingstone, D. M., Sommaruga, R., Straile, D., Van Donk, E., Weyhenmeyer, G. A., and Winderl, M.: Lakes as sentinels of climate change. Limnol Oceanogr., 54, 6, 2283-2297, https://doi.org/10.4319/lo.2009.54.6_part_2.2283, 2009.

Brown, L. C. and Duguay, C. R.: The response and role of ice cover in lake-climate interactions. Progress in Physical Geography, 34, 5, 671-704, https://doi.org/10.1177/0309133310375653, 2010.

Climate Change Initiative Lakes: https://climate.esa.int/en/projects/lakes, last access: 23 June 2023.

Databoks Grønland: https://dataforsyningen.dk/data, last access: 2023.

Delaunay, B. N.: Sur la sphère vide. Bulletin of Academy of Sciences of the USSR, 7, 6, 793–800, 1934.

https://doi.org/10.5194/egusphere-2023-1762
Preprint. Discussion started: 2 August 2023

Duguay, C. R., Bernier, M., Gauthier, Y., and Kouraev, A.: Remote sensing of lake and river ice, in: Remote Sensing of the Cryosphere, First Edition, edited by: Tedesco, M., John Wiley & Sons, Hoboken, New Jersey, 273-306, https://doi.org/10.1002/9781118368909.ch12, 2015.

Earth Engine Code Editor: https://code.earthengine.google.com, last access: 16 April 2023.

Earth Engine Data Catalogue: https://developers.google.com/earth-engine/datasets, last access: 16 April 2023.

Hanna, E., Capellen, J., Fettweis, X., Mernild, S. H., Mote, T. L., Mottram, R., Steffen, K., Ballinger, T. J., and Hall, R. J.: Greenland surface air temperature changes from 1981 to 2019 and implications for ice-sheet melt and mass-balance change, Int J. Climatol., 41, 1336–1352, https://doi.org/10.1002/joc.6771, 2021.

Hock, R., Maussion, F., Marzeion, B., and Nowicki, S.: What is the global glacier ice volume outside the ice sheets?, Journal of Glaciology, 69, 273, 204–210, https://doi.org/10.1017/jog.2023.1, 2023.

Jeffries, M. O., Morris, K., and Duguay, C. R.: Floating ice: lake ice and river ice, in: Satellite Image Atlas of Glaciers of the World – State of the Earth's Cryosphere at the Beginning of the 21st Century: Glaciers, Global Snow Cover, Floating Ice, and Permafrost and Periglacial Environments, edited by: Williams, R. S. and Ferrigno, J. G., U.S. Geological Survey, Reston, Virginia, A381–A424, https://doi.org/10.3133/pp1386, 2012.

Lindenschmidt, K. E., van der Sanden, J., Demski, A., Drouin, H., and Geldsetzer, T.: Characterising river ice along the Lower Red River using RADARSAT-2 imagery, in: CGU HS Committee on River Ice Processes and the Environment, 16th Workshop on River Ice, Winnipeg, Manitoba, 18-22 September 2011, 1-16, 2011.

Magnuson, J. J., Robertson, D. M., Benson, B. J., Wynne, R. H., Livingstone, D. M., Arai, T., Assel, R. A., Barry, R. G., Card V., Kuusisto, E., Granin, N. G., Prowse, T. D., Stewart, K. M., and Vuglinski, V. S.: Historical Trends in Lake and River Ice Cover in the Northern Hemisphere, Science, New Series, 289, 5485, 1743-1746, https://doi.org/10.1126/science.289.5485.1743, 2000.

Murfitt, J. and Duguay, C. R.: Assessing the Performance of Methods for Monitoring Ice Phenology of the World's Largest High Arctic Lake Using High-Density Time Series Analysis of Sentinel-1 Data, Remote Sens., 12, 3, 382, 1-25, https://doi.org/10.3390/rs12030382, 2020.

Murfitt, J. and Duguay, C. R.: 50 years of lake ice research from active microwave remote sensing: Progress and prospects, Remote Sensing of Environment, 264, 112616, 1-21 https://doi.org/10.1016/j.rse.2021.112616, 2021.

Moreira, A., Prats-Iraola, P., Younis, M., Krieger, G., Hajnsek, I., and Papathanassiou, K. P.: A tutorial on synthetic aperture radar, IEEE Geoscience and Remote Sensing Magazine, 1, 1, 6-43, https://doi.org/10.1109/MGRS.2013.2248301, 2013.

Noël, B., van de Berg, W. J., van Wessem, J. M., van Meijgaard, E., van As, D., Lenaerts, J. T. M., Lhermitte, S., Munneke, P. K., Smeets, C. J. P. P., van Ulft, L., van de Wal, R. S. W., and van den Broeke: Modelling the climate and surface mass balance of polar ice sheets using RACMO2 – Part 1: Greenland (1958–2016), The Cryosphere, 12, 811–831, https://doi.org/10.5194/tc-12-811-2018, 2018.

https://doi.org/10.5194/egusphere-2023-1762
Preprint. Discussion started: 2 August 2023

Prowse, T., Alfredsen, K., Beltaos, S., Bonsal, B. R., Bowden, W. B., Duguay, C. R., Korhola, A., McNamara, J., Vincent, W. F., Vuglinsky, V., Walter Anthony, K. M., and Weyhenmeyer, G. A.: Effects of Changes in Arctic Lake and River Ice, AMBIO 2011, 40, 63–74, https://doi.org/10.1007/s13280-011-0217-6, 2011.

Saros, J. E., Anderson, N. J., Juggins, S., McGowan, S., Yde, J. C., Telling, J., Bullard, J. E., Yallop, M. L., Heathcote, A. J., and Burpee, B. T.: Arctic climate shifts drive rapid ecosystem responses across the West Greenland landscape, Environ. Res. Lett., 14, 074027, 1-11, https://doi.org/10.1088/1748-9326/ab2928, 2019.

Sentinel-1: https://sentinel.esa.int/web/sentinel/missions/sentinel-1, last access: 16 April 2023.

Sentinel-1 Algorithms: https://developers.google.com/earth-engine/guides/sentinel1#metadata-and-filtering, last access: 26 June 2023.

Sentinel-1 SAR Technical Guide. https://sentinels.copernicus.eu/web/sentinel/technical-guides/sentinel-1-sar, last access: 16 April 2023.

Sentinel-1 SAR User Guide: https://sentinel.esa.int/web/sentinel/user-guides/sentinel-1-sar, last access: 16 April 2023.

Siles, G., Leconte, R., and Peters D. L.: Retrieval of Lake Ice Characteristics from SAR Imagery, Canadian Journal of Remote Sensing, 48, 3, 379–399, https://doi.org/10.1080/07038992.2022.2042227, 2022.

Stonevicius, E., Uselis, G., and Grendaite, D.: Ice Detection with Sentinel-1 SAR Backscatter Threshold in Long Sections of Temperate Climate Rivers, Remote Sensing, 14, 1627, 1-20, https://doi.org/10.3390/rs14071627, 2022.

Styrelsen for Dataforsyning og Infrastruktur: Åbent Land Grønland [data set], https://dataforsyningen.dk/data/4771, 2023.

The Sentinel-1 Toolbox: https://sentinel.esa.int/web/sentinel/toolboxes/sentinel-1, last access: 26 June 2023.

Tom, M., Aguilar, R., Imhof, P., Leinss, S., Baltsavias, E., and Schindler, K.: Lake Ice Detection from Sentinel-1 SAR with Deep Learning, in: ISPRS Annals of the Photogrammetry, Remote Sensing and Spatial Information Sciences, Volume V-3-2020, XXIV ISPRS Congress, Nice, France, 31 August-02 September 2020, 1-8, https://doi.org/10.5194/isprs-annals-V-3-2020-409-2020, 2020.

United Nations: Transforming our world: The 2030 Agenda for Sustainable Development., United Nations, New York, New York, 41 pp., 2015.

Unterschultz, K. D., van der Sanden, J., and Hicks, F. E.: Potential of RADARSAT-1 for the monitoring of river ice: Results of a case study on the Athabasca River at Fort McMurray, Canada, Cold Regions Science and Technology, 5, 238-248, https://doi.org/10.1016/j.coldregions.2008.02.003, 2009.

U.S./Japan ASTER Science Team: ASTGTM v003, ASTER Global Digital Elevation Model 1 arc second [data set], https://doi.org/10.5067/ASTER/ASTGTM.003, 2023.

Weyhenmeyer, G. A., Meili, M., and Livingstone, D. M.: Nonlinear temperature response of lake ice breakup, Geophysical Research Letter, 31, 7, 1-4, https://doi.org/10.1029/2004GL019530, 2004.

Williams, G., Layman, K. L., Stefan, H. G.: Dependence of lake ice covers on climatic, geographic and bathymetric variables, Cold Regions Science and Technology, 40, 145-164, https://doi-org/10.1016/j.coldregions.2004.06.010, 2004.

https://doi.org/10.5194/egusphere-2023-1762
Preprint. Discussion started: 2 August 2023

Williams, G. and Stefan, H. G.: Modeling of Lake Ice Characteristics in North America Using Climate, Geography, and Lake Bathymetry, Journal of Cold Regions Engineering, 20, 4, 140-167, https://doi-org/10.1061/(asce)0887-381x(2006)20:4(140), 2006.

Woolway, R. I., Kraemer, B. M., Lenters, J. D., Merchant, C. J., O'Reilly, C. M., Sharma, S.: Global lake responses to climate change, Nat Rev Earth Environ, 1, 388–403, https://doi.org/10.1038/s43017-020-0067-5, 2020.

World Meteorological Organization (WMO), United Nations Educational, Scientific and Cultural Organization, Intergovernmental Oceanographic Commission, United Nations Environment Programme, International Science Council (ISC): The 2022 GCOS Implementation Plan (GCOS-244), WMO, Geneva, Switzerland, 98 pp., 2022a.

World Meteorological Organization (WMO), United Nations Educational, Scientific and Cultural Organization, Intergovernmental Oceanographic Commission, United Nations Environment Programme, International Science Council (ISC): The 2022 GCOS ECVs Requirements (GCOS-245), WMO, Geneva, Switzerland, 98 pp., 2022b.

https://doi.org/10.5194/egusphere-2023-1762
Preprint. Discussion started: 2 August 2023

Appendix A

Table A1: Number of lakes through the different analysis steps in our study as well as their relative coverage compared to the entire lake inventory. We found that only lakes in S, SW and NW Greenland are suitable to perform a spatio-temporal analysis of break-up timings and a statistical analysis considering climatological data. [1] lakes with suitable temporal and radiometric characteristics for the automated lake ice break-up detection algorithm, [2] lakes used for spatio-temporal analysis, [3] lakes used for analysis of excess radiation, energy and cumulative PDDs, [4] lakes used for upscaled results of excess energy.

		inventory	A ≥ 0.1 km²	after pre-processing [1]	with all DOYs detected	after outlier removal[2]	with climate data[3]	upscaled excess energy[4]
all lakes	abs.	155870	14336	1693	828	563	491	100486
N		18631	1613	4	3	0	0	0
NE		19363	1973	1	1	0	0	0
SE		8402	547	2	0	0	0	0
S		11301	792	54	33	21	21	11301
SW		79147	7667	1360	640	450	406	79147
NW		19013	1741	272	151	92	64	10024
all lakes	rel.	100.0%	10.0 %	1.1 %	0.5 %	0.4 %	0.3 %	64.5 %
N		12.0%	1.0 %	< 0.1 %	< 0.1 %	0.0 %	0.0 %	0.0 %
NE		12.4%	1.3 %	< 0.1 %	< 0.1 %	0.0 %	0.0 %	0.0 %
SE		5.4%	0.4 %	< 0.1 %	0.0 %	0.0 %	0.0 %	0.0 %
S		7.3%	0.5 %	< 0.1 %	< 0.1 %	< 0.1 %	< 0.1 %	7.3 %
SW		50.8%	4.9 %	0.9 %	0.4 %	0.3 %	0.3 %	50.8 %
NW		12.2%	1.1 %	0.2 %	0.1 %	0.1 %	0.0 %	6.4 %

https://doi.org/10.5194/egusphere-2023-1762
Preprint. Discussion started: 2 August 2023

Table A2: Surface area [km²] of lakes through the different analysis steps in our study as well as their relative coverage compared to the entire lake inventory. We found that only lakes in S, SW and NW Greenland are suitable to perform a spatio-temporal analysis of break-up timings and a statistical analysis considering climatological data. [1] lakes with suitable temporal and radiometric characteristics for the automated lake ice break-up detection algorithm, [2] lakes used for spatio-temporal analysis, [3] lakes used for analysis of excess radiation, energy and cumulative PDDs, [4] lakes used for upscaled results of excess energy.

		inventory	A ≥ 0.1 km²	after pre-processing [1]	with all DOYs detected	after outlier removal[2]	with climate data[3]	upscaled excess energy[4]
all lakes	abs.	14183	11879	2770	1485	971	925	8806
N		2165	1876	12	12	0	0	0
NE		2198	1896	36	36	0	0	0
SE		372	260	11	0	0	0	0
S		570	416	29	18	15	15	570
SW		7381	6214	2310	1148	810	788	7380
NW		1497	1217	372	271	146	122	854
all lakes	rel.	100.0 %	83.8 %	19.5 %	10.5 %	6.8 %	6.5 %	62.1 %
N		15.3 %	13.2 %	0.1 %	0.1 %	0.0 %	0.0 %	0.0 %
NE		15.5 %	13.4 %	0.3 %	0.3 %	0.0 %	0.0 %	0.0 %
SE		2.6 %	1.8 %	0.1 %	0.0 %	0.0 %	0.0 %	0.0 %
S		4.0 %	2.9 %	0.2 %	0.1 %	0.1 %	0.1 %	4.0 %
SW		52.0 %	43.8 %	16.3 %	8.1 %	5.7 %	5.6 %	52.0 %
NW		10.6 %	8.6 %	2.6 %	1.9 %	1.0 %	0.9 %	6.0 %

https://doi.org/10.5194/egusphere-2023-1762
Preprint. Discussion started: 2 August 2023

Appendix B

Table A3: Lake ice break-up validation from time-lapse cameras (Abermann et a.l, 2019) in SW Greenland.

year	Badesø Lake ID: 16515 13 m a.s.l.			Langesø Lake ID: 17830 21 m a.s.l			Quassi-sø Lake ID: 17831 226 m a.s.l.			yearly mean error	**overall mean error**
	DOY val.	DOY S1	diff.	DOY val.	DOY S1	diff.	DOY val.	DOY S1	diff.		
2017	168	169	1	167	168	1	173	175	2	1	**5**
2018	171	189	18	171	-	-	184	-	-	18	
2019	149	152	3	148	152	4	159	-	-	4	
2020	161	-	-	166	171	5	179	185	6	6	

Table A4: Lake ice break-up validation from observations, thermistor data and satellite imagery of 11 lakes (Saros et al., 2019) in the Kangerlussuaq area compared to 14 lakes from our study close by.

year	median DOY val.	median DOY S1	diff.	**overall mean difference**
2017	155	162	7	**5**
2018	164	169	5	
2019	139	144	5	
2020	150	154	4	
2021	150	153	3	

Table A5: Lake ice break-up validation from ESA CCI data (Climate Change Initiative Lakes, 2023) in SW Greenland.

year	Lake ID: 70398 519 m a.s.l.			Lake ID: 70316 707 m a.s.l			yearly mean error	**overall mean error**
	DOY val.	DOY S1	diff.	DOY val.	DOY S1	diff.		
2017	177	181	4	172	175	3	4	**2**
2018	199	199	0	199	201	2	1	
2019	160	165	5	159	160	1	3	
2020	182	184	2	183	184	1	2	

https://doi.org/10.5194/egusphere-2023-1762
Preprint. Discussion started: 2 August 2023

Appendix C

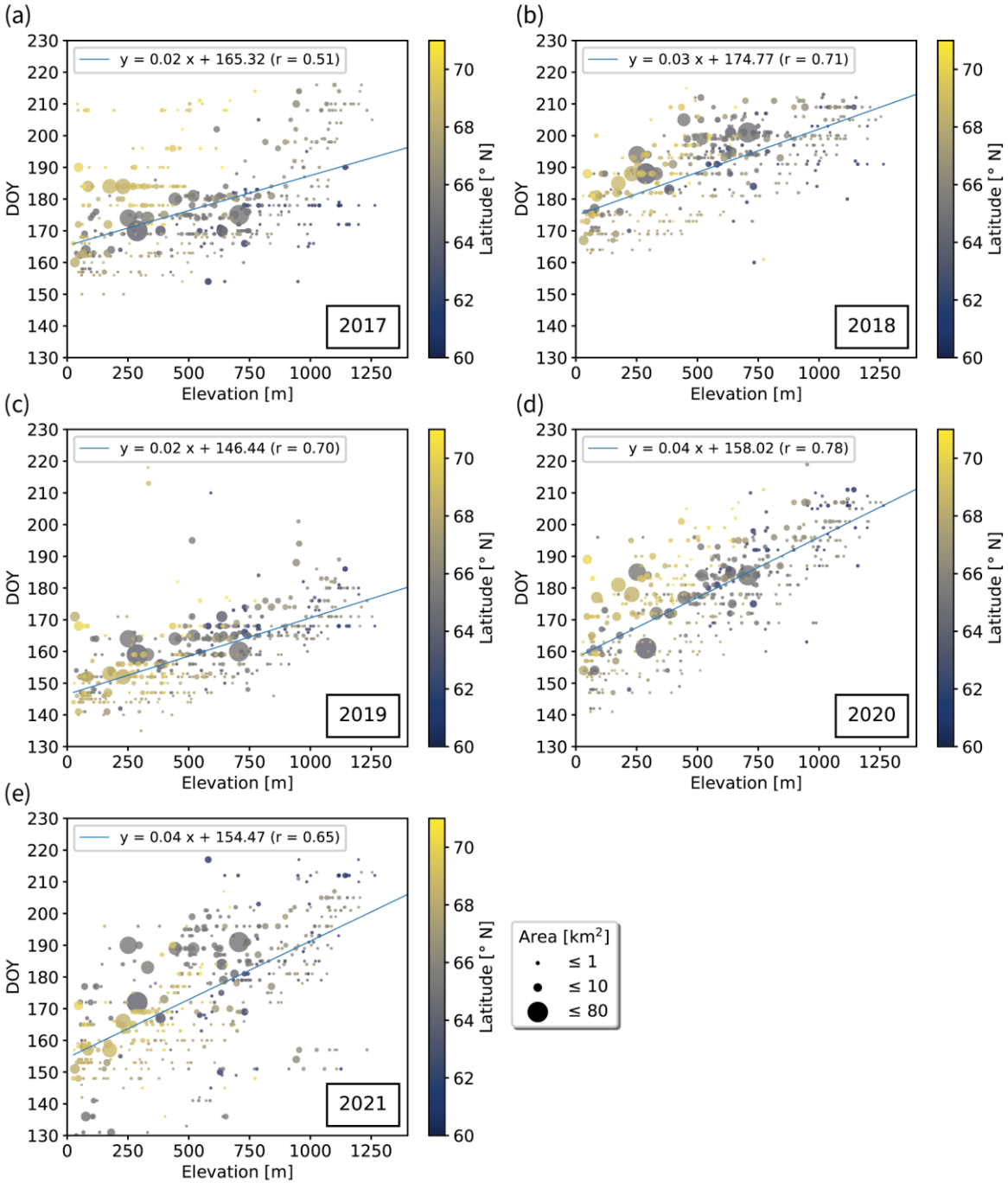

Figure C1: Lake ice break-up timings vs elevation for the years (a) 2017 to (e) 2021. Break-up dates increase by 2-4 DOY per 100 m elevation gain exhibiting strong correlations ($0.51 \leq r \leq 0.78$).

https://doi.org/10.5194/egusphere-2023-1762
Preprint. Discussion started: 2 August 2023

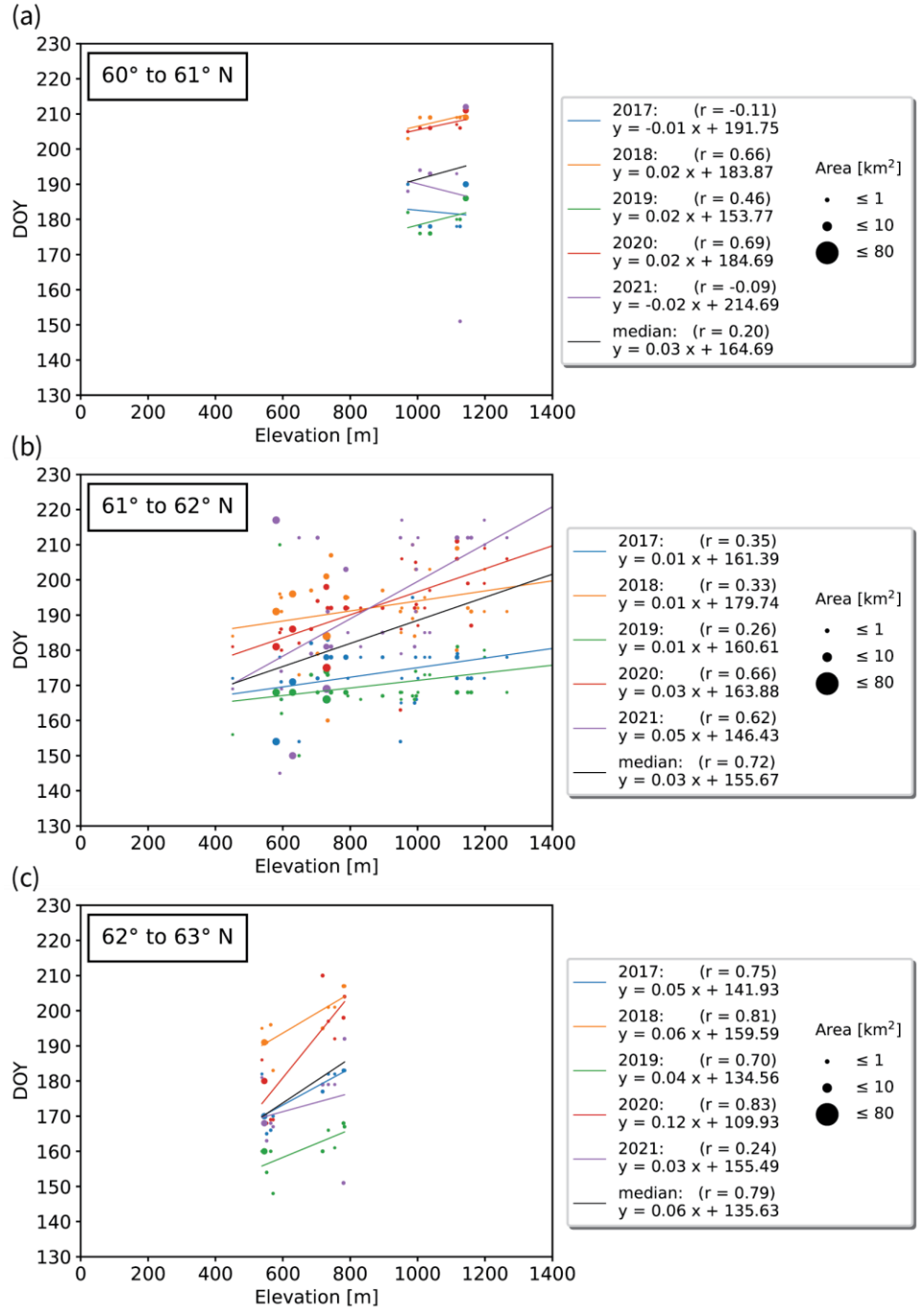

Figure C2: (a)-(c) Yearly lake ice break-up timings vs elevation grouped by 1° latitude between 60° and 63° N. Several years exhibit strong correlations between break-up timing and elevation which increase by 3-6 days per 100 m elevation gain.

https://doi.org/10.5194/egusphere-2023-1762
Preprint. Discussion started: 2 August 2023

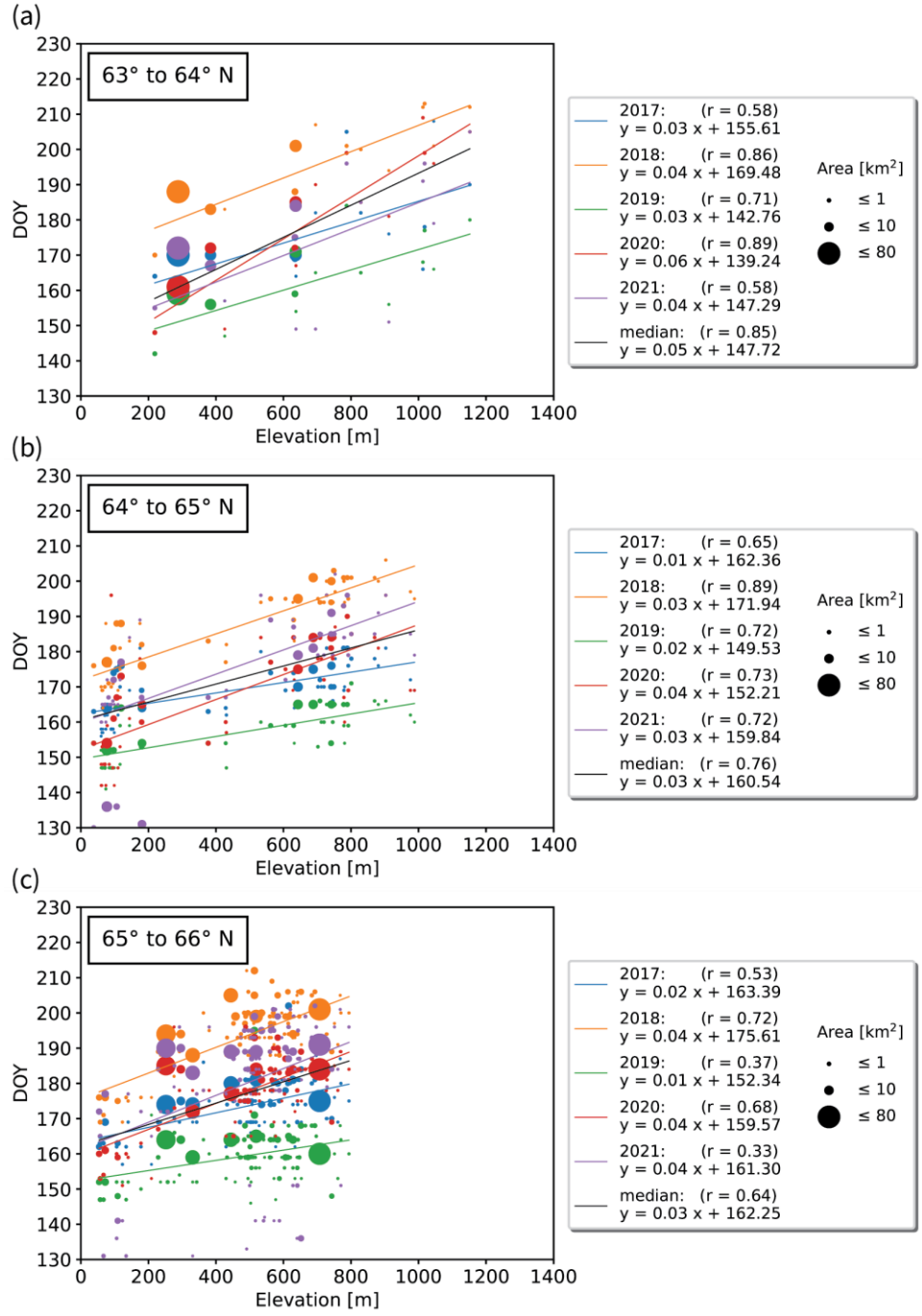

Figure C3: (a)-(c) Yearly lake ice break-up timings vs elevation grouped by 1° latitude between 63° and 66° N. Several years exhibit strong correlations between break-up timing and elevation which increase by 3-6 days per 100 m elevation gain.

https://doi.org/10.5194/egusphere-2023-1762
Preprint. Discussion started: 2 August 2023

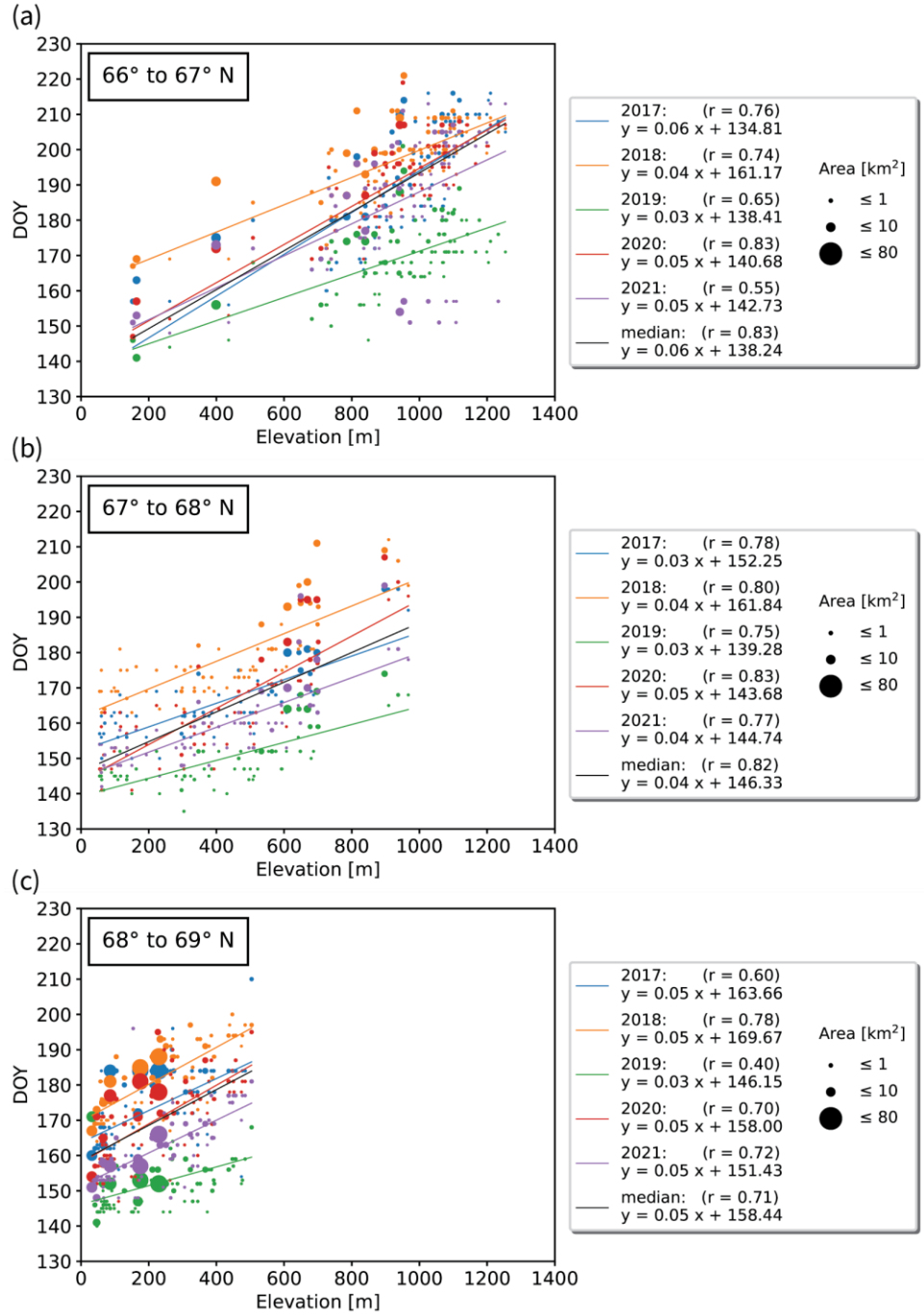

Figure C4: (a)-(c) Yearly lake ice break-up timings vs elevation grouped by 1° latitude between 66° and 69° N. Several years exhibit strong correlations between break-up timing and elevation which increase by 3-6 days per 100 m elevation gain.

https://doi.org/10.5194/egusphere-2023-1762
Preprint. Discussion started: 2 August 2023

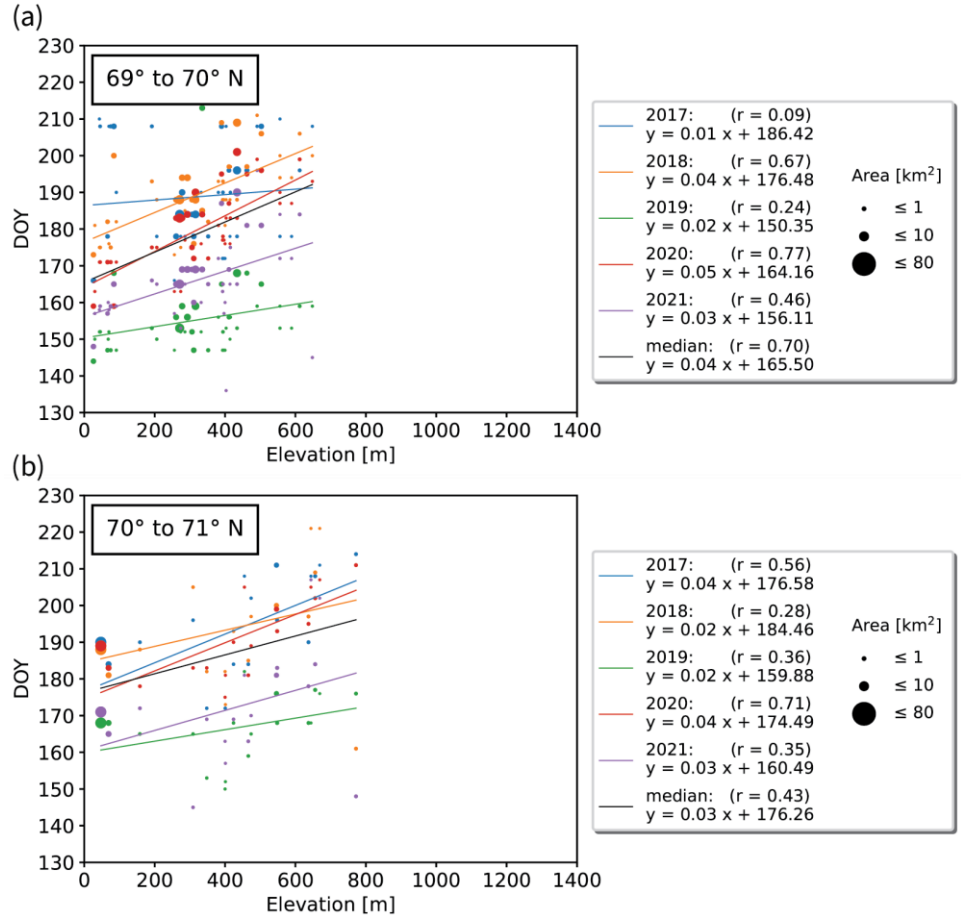

Figure C5: (a)-(c) Yearly lake ice break-up timings vs elevation grouped by 1° latitude between 69° and 71° N. Several years exhibit strong correlations between break-up timing and elevation which increase by 3-5 days per 100 m elevation gain.

https://doi.org/10.5194/egusphere-2023-1762
Preprint. Discussion started: 2 August 2023

Appendix D

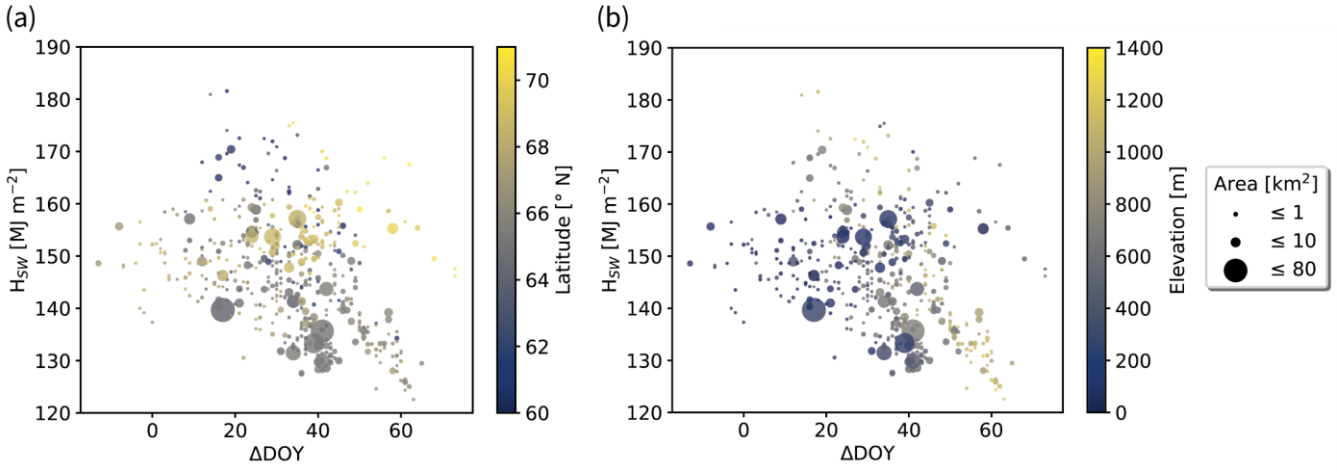

Figure D1: Excess radiation H_{SW} due to lake-specific break-up timings which are 8 days earlier compared to the median break-up timings for the period 2017 to 2021 vs the time lag between the date of maximum incoming solar radiation and median lake ice break-up (ΔDOY) with color signatures for (a) latitude and (b) elevation. The median value of ΔDOY for the studied lakes amounts to 35 days (i.e., the lake-specific median break-up timing being 35 days after the solar radiation maximum).

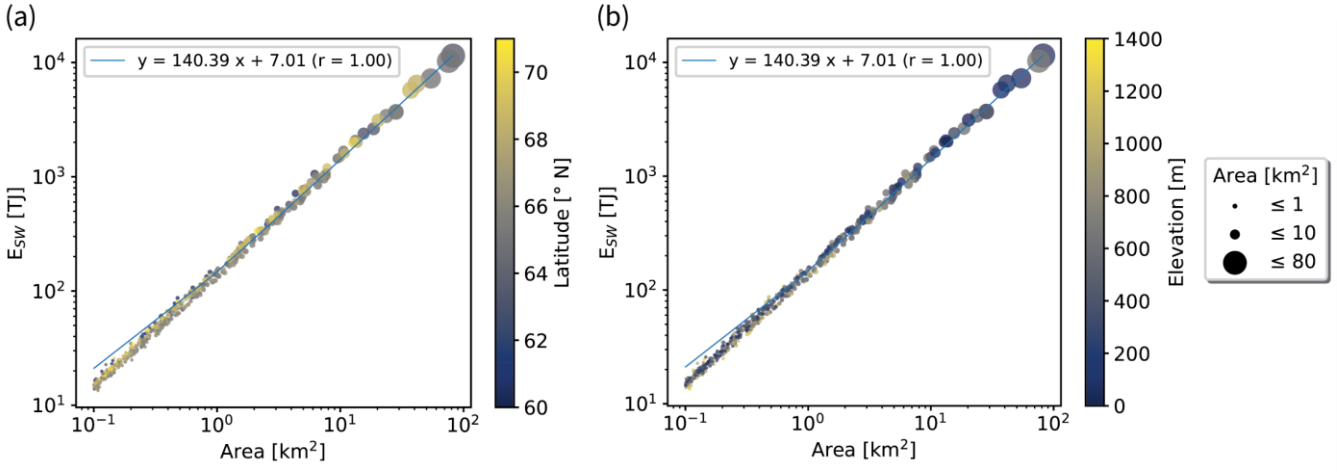

Figure D2: Excess energy E_{SW} due to lake-specific break-up timings which are 8 days earlier compared to the median break-up timings for the period 2017 to 2021 vs lake surface area with color signatures for (a) latitude and (b) elevation. Lake surface areas strongly determine E_{SW} values explaining more than 99 % of the variability in E_{SW}.